Journal of Aerosol Science xxx (xxxx) 106243

Contents lists available at ScienceDirect

Journal of Aerosol Science

journal homepage: www.elsevier.com/locate/jaerosci

Computational study of the ECN spray C via one-way coupling of internal nozzle flow and ensuing spray

Hengjie Guo *, Roberto Torelli

Center for Advanced Propulsion and Power, Argonne National Laboratory, Lemont, IL, 60439, USA

ARTICLE INFO

Handling Editor: Chris Hogan

Keywords:
Nozzle flow
Cavitation
Injection modeling
One-way coupling
ECN Spray C injector

ABSTRACT

In this study, computational fluid dynamics simulations of the Engine Combustion Network Spray C injector were performed to investigate the effect of the internal nozzle flow on the development of the ensuing spray in automotive fuel injectors. A set of simulation best practices was first developed to achieve an accurate representation of the internal nozzle flow. Detailed, spatiotemporally defined information was extracted at the injector's orifice exit and stored in maps that were subsequently employed to initialize a Lagrangian spray by means of a static, one-way coupling (OWC) approach. To highlight the impact of the in-nozzle flow on the spray, the OWC approach was compared with the conventional rate-of-injection (ROI) approach, for which the spray parcels are commonly initialized using a blob injection model. The results indicated that, using the ROI approach, considerable evaporation was observed within the plume in the near-nozzle region. On the other hand, the OWC approach showed evidence of evaporation farther downstream and at the plume periphery. The different behavior observed with the two approaches was mostly due to substantial differences in fuel mass distribution. The liquid fuel concentration predicted by the OWC approach matched well with X-ray tomography measurements of projected fuel mass per unit volume, in terms of both magnitude and distribution. In contrast, an unphysical distribution of fuel mass characterized by an extremely low liquid concentration was predicted by the ROI approach. In the far-field, the effect of the in-nozzle flow was found to be weaker as the spray penetrated and interacted with the ambient gas. In this region, the OWC and ROI approaches provided similar predictions of vapor penetration, spray morphology, and mixing-related characteristics.

1. Introduction

Compression ignition engines are extensively used in the transportation sector due to their performance in terms of thermal efficiency, power output, and durability. While new alternatives such as electric and fuel cell vehicles are being developed and become more mature, the use of compression ignition engines in combination with carbon-free fuels is regarded as one practical way to achieve effective decarbonization in heavy-duty transport in the short term (Abbasi & Abbasi, 2011; Duan et al., 2021). In order to meet the increasingly more stringent emission legislations for NO_x and particulate matter, recent research on compression ignition engines focused on the development of advanced combustion techniques such as homogeneous charge compression ignition (Yao et al., 2009), premixed charge compression ignition (Kanda et al., 2005), and reactivity controlled compression ignition (Reitz &

* Corresponding author.
E-mail addresses: hengjie.guo@anl.gov (H. Guo), rtorelli@anl.gov (R. Torelli).

https://doi.org/10.1016/j.jaerosci.2023.106243
Received 15 May 2023; Received in revised form 20 July 2023; Accepted 22 July 2023
0021-8502/© 20XX

Duraisamy, 2015), with the overarching goal of achieving low-temperature combustion (LTC) to inhibit the chemistry of NO_x and soot formation and reduce such emissions.

The performance of LTC in compression ignition engines relies on the ability of the fuel injection systems to create the conditions for the desired combination of fuel/air mixture at the desired timing (Krishnamoorthi et al., 2019; Peng et al., 2022). The pressure gradient that is established between the upstream rail and the downstream combustion chamber drives the fuel across the injector and defines the near-nozzle flow field as a combination of several factors: injection and chamber conditions, interaction between the liquid fuel and the moving parts of the injector internal geometry, and physical properties of the fuel itself. In this last decade, significant research has been carried out on the numerical modeling of internal and near-nozzle injection flows, enhanced by the development of non-destructive experimental techniques and increased availability of high-performance computing. The accurate reproduction of the physics occurring inside (Baldwin et al., 2016; Chen et al., 2018) and immediately outside (Battistoni et al., 2018, 2019) of the injector can provide useful insights into the development of the ensuing spray and how it interacts with the local environment.

A classic topic of interest in the study of in-nozzle flows is cavitation, which is the local phase change caused by a sudden and sustained pressure decrease occurring inside the injector (Andriotis et al., 2008). Cavitation typically occurs at the needle seat and at the inlet of the injector orifices where strong velocity and pressure gradients are more likely to develop. The presence of cavitation results in perturbations to the internal flow field and significantly affects the flow characteristics such as mass flow rate, spatial mass distribution, etc. (Payri et al., 2004), which subsequently influences the spray characteristics including the liquid penetration and Sauter mean diameter (Sou et al., 2007). To understand the impact of in-nozzle cavitation on the injection process, the Engine Combustion Network (ECN) proposed the "Spray C″ injector, a single-hole research-grade diesel injector characterized by a sharp orifice inlet and a diverging orifice which facilitate flow separation (Engine Combustion Network, 2023). To date, much experimental research has been reported in the literature that aims to characterize several aspects of the Spray C injector, including injection rate (Payri et al., 2016), in-nozzle flow patterns (Tekawade et al., 2020), spray characteristics (Gimeno et al., 2016), and combustion characteristics (Maes et al., 2020). Similarly, computational fluid dynamics (CFD) studies have been carried out to study the flow and spray characteristics both inside (Guo et al., 2020a) and outside (Bao et al., 2022) the injector. These studies indicated that the sharp orifice inlet of the Spray C injector induced strong in-nozzle cavitation which eventually resulted in partial hydraulic flip and caused considerable flow asymmetry at the orifice exit and immediately downstream. On the other hand, the study by Bao et al. (2022) demonstrated that the blob injection model which assumes symmetric sprays achieved promising results against experiments when simulating the ECN Spray C, suggesting that the asymmetry of the nozzle flow may have limited effects on the development of the spray in the far-field.

The goal of this study is to investigate the effect that the in-nozzle flow characteristics of the Spray C injector have on the development of the ensuing spray by means of high-fidelity CFD simulations. A static coupling approach known as one-way coupling (OWC) and developed by Quan et al. (2016) was employed to couple the Eulerian in-nozzle flow simulations with the Lagrangian spray simulations. The in-nozzle flow was simulated first to generate accurate flow information at the orifice exit. This time- and space-resolved information was stored into spatiotemporally defined maps and used with the spray simulations to initialize the spray parcels. To demonstrate the effect of the in-nozzle flow, the OWC results were compared against those obtained with the conventional rate-of-injection (ROI) approach, in which the details of the in-nozzle flow are not considered. More information about the OWC approach can be found in the work of Quan et al. (2016) and Torelli et al. (2022).

The manuscript is organized as follows: first, a description of the Spray C injector and the target operating conditions is provided. A section dedicated to the computational framework follows, in which details about the Eulerian nozzle flow modeling, the Lagrangian spray modeling, and the injection modeling methods are introduced. In the next section, the results from the in-nozzle flow simulations are presented, with a focus on the definition of simulation best practices developed to capture the transient and quasi-steady-state nozzle flow characteristics. Finally, the results from the Lagrangian spray simulations using the OWC and ROI approaches are analyzed to understand and explain the effect of the in-nozzle flow on the ensuing spray. At the end of the discussion, the key takeaway points of this work are summarized.

2. Injector specifications and operating conditions

The ECN Spray C injector is a single-hole diesel injector with an axial orifice (Engine Combustion Network, 2023). Fig. 1(a) shows a cross-section of the internal geometry of the specific injector unit used in this work (part no. 210037), which was reconstructed from X-ray tomography measurements performed at the Advanced Photon Source at Argonne National Laboratory (Argonne). The Spray C

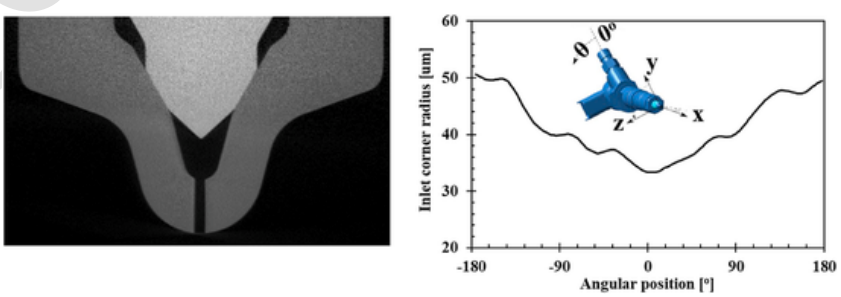

Fig. 1. Cross-sectional image of the X-ray-scanned geometry (left) and orifice inlet radius (right) of the ECN Spray C injector (part no. 210037).

is designed to resemble typical heavy-duty engine injector dimensions, and it has a relatively large orifice inlet diameter of 0.185 mm. The orifice has a diverging development which results in a K-factor of −2.5 and was intentionally manufactured in such way to facilitate strong cavitation within the orifice. Fig. 1(b) defines the reference system used in this study and plots the curvature radius of the orifice inlet as a function of the angular position. The orifice features an asymmetrical geometry and a sharp inlet, with a minimum inlet curvature radius of 33 μm. The geometrical details of the injector are summarized in Table 1.

N-dodecane, a typical single-component surrogate for diesel fuel (Pitz & Mueller, 2011), was used as the working fluid. The injection pressure was 150 MPa, and the injection duration was 1.50 ms. The injector and fuel temperature were 363 K. The fuel was discharged into a chamber filled with nitrogen gas at a temperature of 900 K and a pressure of 6.0 MPa, creating an evaporative environment that is representative of realistic injection conditions in diesel engines. As nitrogen was used as the ambient gas, no chemical reactions are expected in this study. The operating conditions are summarized in Table 2.

3. Computational setup

Two sets of simulations were performed in this study. The first one addressed the in-nozzle flow simulations carried out within a fully Eulerian framework. The second set focused on the spray simulations conducted via a discrete droplet modeling approach within a Lagrangian framework. The details of the computational setup are discussed below. Note that all the simulations in this study were realized using the CFD code CONVERGE v3.0 (Richards et al., 2022), and were run on the high-performance Laboratory Computing Resource Center (LCRC) clusters at Argonne.

3.1. Eulerian nozzle flow modeling

The liquid-gas two-phase flow inside the nozzle was described via a single-fluid mixture model, which assumes strong coupling between the phases and a barycentric value of velocity and thermodynamic state to be accounted for in the transport equations (Leung, 1986). The homogeneous relaxation model proposed by Bilicki and Kestin (1990) was used to determine the phase change due to cavitation, which describes the evolution of instant vapor quality by means of a first-order relaxation towards the equilibrium value. The model constants proposed by Downar-Zapolski et al. (1996) were employed. A large eddy simulation framework with the one-equation dynamic structure model (Pomraning, 2001) was used to solve the larger turbulent structures and model the effects of the sub-grid scale turbulence. The gas species were described via the Redlich-Kwong equation-of-state (EOS) (Redlich & Kwong, 1949), while the liquid phase was modeled as compressible using an exponential barotropic fluid assumption.

The realistic nozzle geometry shown in Fig. 1 was utilized in the nozzle flow simulations. The 3-D needle motion profile obtained via X-ray phase-contrast imaging under the test condition was used as an input, which is shown in Fig. 2. The simulations were run using a density-based transient solver for a simulated duration of 1.6 ms. The mesh size at the orifice was set at 10 μm. A variable minimum-mesh-size strategy based on the gap between the needle and the seat was used to account for the needle off-axis displacement during the injection event, as reported by Guo et al. (2020a). This mesh strategy resulted in a peak cell count of 6.4 million. A variable time-step formulation was used, controlled by a convection Courant-Friedrichs-Lewy (CFL) number of 0.4. The spatial discretization was achieved with a second-order central difference scheme.

Table 1
Geometrical details of the ECN Spray C injector (part no. 210037).

Parameter	Value	Units
Hole inlet diameter	0.185	[mm]
Hole outlet diameter	0.210	[mm]
K-factor	−2.5	[−]
Orifice length	1.0	[mm]
L/D ratio	5.3	[−]

Table 2
Summary of the operating conditions.

Parameter	Value	Units
Fuel	N-dodecane	[−]
Ambient gas	Nitrogen	[−]
Injection pressure	150	[MPa]
Injection temperature	363	[K]
Injection duration	1.5	[ms]
Ambient temperature	900	[K]
Ambient pressure	6.0	[MPa]

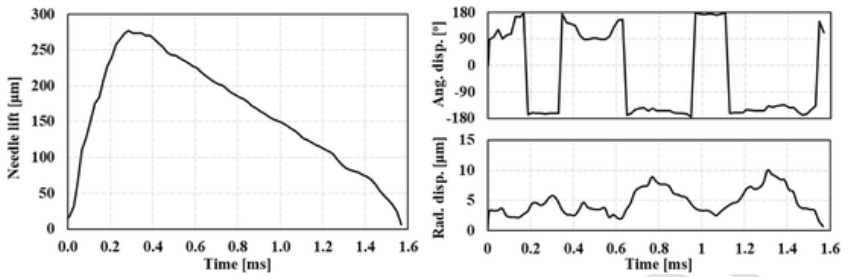

Fig. 2. 3-D needle motion profiles used in the nozzle flow simulations (left: needle lift; right: off-axis displacement).

3.2. Lagrangian spray modeling

The evolution of the spray was modeled via the discrete droplet modeling approach proposed by Dukowicz (1980). This approach relies on a Lagrangian formulation that uses statistical entities called parcels to model the likelihood that liquid droplets characterized by the same characteristics (e.g., diameter, temperature, density, etc.) are located in a certain area of the computational domain. The Kelvin/Helmholtz-Rayleigh/Taylor model (Reitz & Beale, 1999) was used to model the primary breakup and atomization processes. The O'Rourke model (Amsden et al., 1989) and the Frössling model (Amsden et al., 1997) were employed for considerations of droplet turbulent dispersion and droplet evaporation, respectively. The turbulence model and gaseous EOS were kept identical to those used for the in-nozzle flow simulations. The liquid phase was modeled as incompressible due to the relatively stable pressure in the chamber.

The computational domain of the Lagrangian spray simulation was modeled as a cylinder with diameter of 50 mm and length of 100 mm. The base mesh size was set at 1.0 mm. Four levels of adaptive mesh refinement, which resulted in a minimum mesh size of 62.5 μm, were enabled wherever the local fluctuations of velocity and temperature exceeded 0.1 m/s and 1.0 K, respectively. A fixed embedding of 62.5 μm was employed in a conical region near the orifice, extending 7.0 mm downstream of the injector tip. The simulations were run using a density-based transient solver for a simulated duration of 1.0 ms. The resulting peak cell count in the simulations was approximately 25 million. The spatial discretization was achieved with a second-order central difference scheme. A variable time-step algorithm was used with a maximum CFL number of 0.4.

3.3. Injection modeling methods

The injection of Lagrangian parcels was modeled via two different approaches. The first is the conventional ROI approach in which the parcels, initialized via the blob injection model (Reitz, 1987), present an initial droplet size that is equal to the effective orifice diameter, i.e., 185 μm. The initial droplet velocity was calculated based on the discharge coefficient and the rate-of-injection profile obtained from Payri et al. (2016). A spray spreading angle of 21.0° was used to determine the direction of the velocity vectors, measured by experiments under the same test condition (Gimeno et al., 2016).

The second approach to model the injection process is a one-way coupled method developed by Quan et al. (2016), which enables the definition of the initial parcel properties in terms of mass, momentum, and temperature based on Eulerian in-nozzle flow simulations. Over a user-defined surface, in this case the orifice exit, a time- and space-resolved map of the two-phase flow characteristics is generated. Each computational cell of the map represents a parcel injection location if the local value of the liquid volume fraction exceeds a user-defined threshold, set to 0.1 for this study in accordance with the results of Saha et al. (2017). The diameter of the injected droplets depends on the nozzle diameter and the area coefficient, and the injected mass is determined by the results of the Eulerian in-nozzle flow simulation. The continuity is ensured by the number of droplets per parcel, which is constrained by a minimum mass value for each parcel that must be matched to allow injection, while the droplet temperature is mapped from the Eulerian simulations.

The turbulence kinetic energy (TKE) calculated from the Eulerian simulations can be used to add a perturbation to the mapped velocity of the parcels. A reliable simulation of the interaction between the spray and the gas depends on this early disturbance of the parcel velocities because it can enhance air entrainment and the subsequent initial plume expansion within the outer chamber. The considerably larger mesh size used in the Lagrangian spray modeling, along with the lack of gaseous feature initialization at the coupling interface, can generate sudden damping of the TKE values. For this reason, a TKE-based perturbation of the parcel velocities is chosen as the only tuning parameter for the OWC framework, as shown by Nocivelli et al. (2019). An initial TKE value of 8000 m^2/s^2 was employed in this study to add a perturbation to the initial droplet velocities which corresponded to a spreading angle of 21° and allowed for consistency between the OWC and ROI simulations.

4. In-nozzle flow simulations

In a previous study by the authors (Guo et al., 2020a), the in-nozzle flow of the ECN Spray C injector was investigated by combining high-fidelity CFD simulations with state-of-the-art X-ray technology. The simulations predicted promising results against the experiments in terms of characteristics such as in-nozzle flow patterns, cavitation layer thickness, etc. However, as the previous study

mostly focused on the quasi-steady-state behavior, it is necessary to validate the CFD setup in the initial transient of the injection event. Besides, to ensure that reliable boundary conditions are mapped for the Lagrangian spray simulations, further analysis is required to validate the predicted flow characteristics at the orifice exit where the map file is generated.

4.1. Mass flow rate

Although a good match of mass flow rate was achieved during the quasi-steady-state portion of the injection (Guo et al., 2020a), the predicted initial transient differed significantly from the experimental observations. Hence, a parametric study on the CFD setup was conducted, in which two factors were examined, i.e., the effect of minimum needle lift, and the role of the volume fraction of ambient gas in the sac and orifice region. The results of this study are shown in Fig. 3.

Fig. 3(a) indicates the predictions of the in-nozzle flow simulations with different minimum needle lifts. The experimental baseline was obtained from Payri et al. (2016). The minimum needle lift represents the location of the needle when the simulations begins, and determining this value is a trade-off problem. If the minimum needle lift is too high, the initial transient of the nozzle flow cannot be properly reproduced. On the other hand, the minimum needle lift should not be too small in simulations, as it would require a very large number of very small cells to describe a rather short portion of the injection event. Conversely, if relatively large mesh sizes were to be used with very small lifts, the numerical viscosity would be artificially increased due to having too few cells in the gap region between the needle and the seat. The selection of minimum needle lift should be dependent on the mesh size in the gap region, which is 5.0 μm in this study. Three different minimum needle lifts were discussed, i.e., 3.0, 9.0, and 15.0 μm. It is noted that the sac and orifice were filled with 100% gas in the simulations, as it will be discussed later. It is shown that with the minimum needle lift of 15.0 μm, a spike in the mass flow rate was predicted during the initial transient, which was not observed in the experiments. This indicates that the minimum needle lift is likely too high, leading to too much fluid to be flushed through the gap at the beginning of the simulation. The unphysical spike observed for the 15.0 μm case disappeared when the minimum needle lift was reduced to 9.0 μm. When the needle lift was further reduced to 3.0 μm, the predicted mass flow rate was considerably different than the other two cases during the initial transient, due to the fact that only one layer of cells was applied to the gap and the aspect ratio of the cells within the needle-to-seat gap was less than 60% at the beginning of the simulation.

Fig. 3(b) shows the predictions of the in-nozzle flow simulations with different volume fractions of ambient gas initialized in the sac and orifice regions. It is noted that the initial needle lift was 15.0 μm in the simulations. According to recent observations through optical diagnostics (Guo et al., 2020b), the air in the outer chamber could be ingested into the sac region at the end of the injection, forming stagnant air bubbles inside the nozzle which could affect the initial transient of the next injection. To consider this effect from a modeling standpoint, the sac and orifice regions were initialized as a homogeneous mixture of liquid fuel and ambient gas. Three cases with different ambient gas fractions were examined. Case 1 (green curve) represents a fully empty sac and orifice region with 100% of ambient gas. In case 2 (red curve), the sac and orifice were filled with 100% of liquid fuel at the chamber pressure. In case 3 (blue curve), the sac and orifice were filled with 50% of ambient gas in volume. The results indicated that the initialization of the sac and orifice region has a considerable impact on the initial mass flow rate. The simulation results with 50% of ambient gas in the sac and orifice region showed the best match against the experiment data, which aligns with the study of Battistoni et al. (2019).

Based on the learnings from Fig. 3, a simulation best practice was determined with the minimum needle lift of 9 μm and the initial gas volume fraction of 50% in the sac and orifice region. Fig. 4 shows the predicted mass flow rate with this setup and how it compares to the experimental signal. It is demonstrated that the simulation results matched well with the experimental data in both the initial transient and the quasi-steady-state stages, which provides confidence that the droplet parcels will be initialized with the correct momentum in the Lagrangian spray simulations.

4.2. Orifice-exit flow characteristics

The mass flow rate discussed above represents the overall behavior of the in-nozzle flow. To examine the space-resolved flow characteristics at the orifice exit, Fig. 5 illustrates the spatial distribution of fuel mass per unit volume at 0.1 mm downstream of the orifice exit, obtained from experiments and simulations. The experimental data were obtained from the time-resolved X-ray tomography

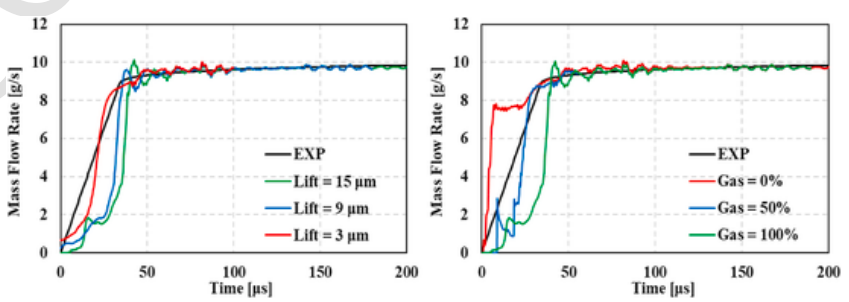

Fig. 3. Effect of minimum needle lift (a) and initial gas volume fraction in the sac and orifice region (b) on the predicted mass flow rate at the initial transient stage.

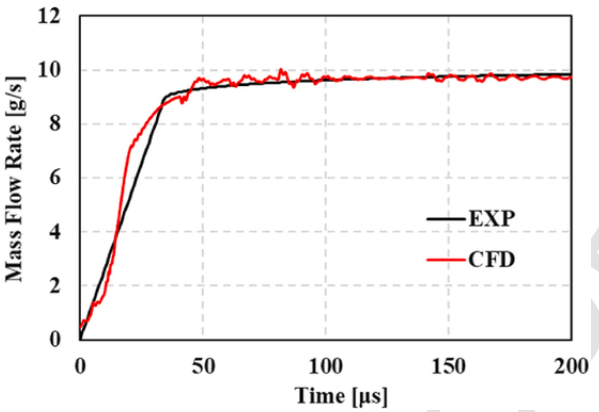

Fig. 4. Predicted mass flow rate with the simulation best practice developed in this study, compared against experimental data.

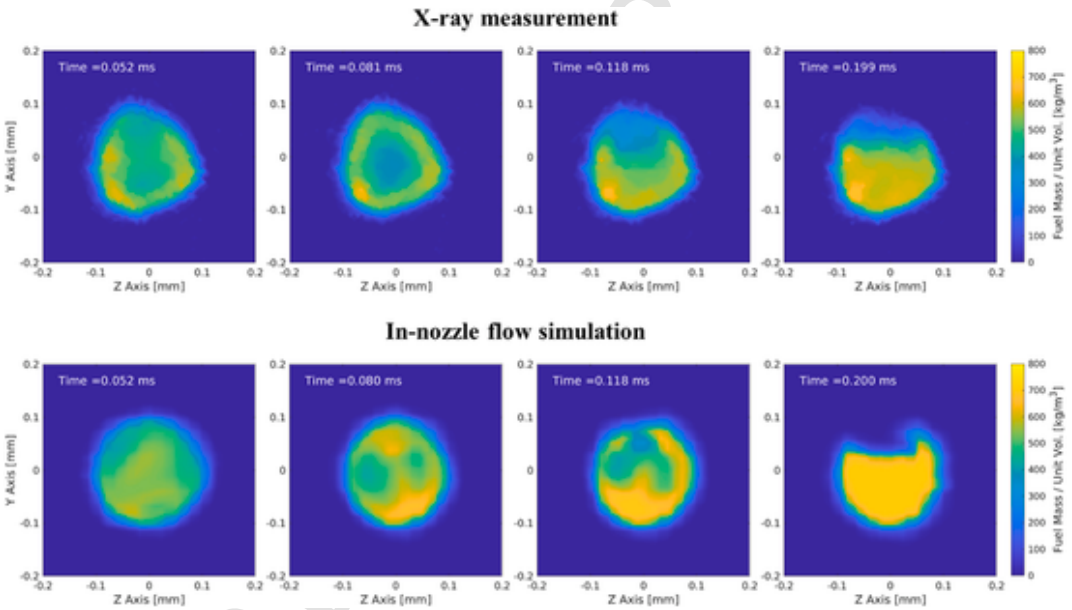

Fig. 5. Measured (top row) and predicted (bottom row) fuel mass per unit volume at 0.1 mm from the orifice exit during the initial transient stage.

measurements reported by Sforzo et al. (2019). It is noted that the experiment was performed at the ambient temperature of ~300 K and the ambient pressure of 20 bar, which is different from the conditions in the simulations. However, for internal nozzle flow, the heat exchange between fuel and ambient gas is negligible, and the flow dynamics is mainly driven by the pressure difference, which only changed by 3% under the two conditions. Hence, it is expected that the different ambient pressure and temperature have limited effects on the flow development.

Only the initial transient stage is discussed here. The experimental data showed that the flow through the orifice exit was quasi-circular at the start of the injection (0.052 ms), which was captured by the simulation. At 0.081 ms, a cavity can be vaguely observed forming within the core of the jet. Although the structure of this cavity was not reproduced, two smaller cavities were predicted in the simulations, which indicates that the simulations were able to reflect the transient dynamics qualitatively. The fuel mass per unit volume decreased in the upper half of the orifice at 0.118 ms, indicating the inception of a partial hydraulic flip (Guo et al., 2020a). The flow pattern became relatively stable after 2.00 ms, with the flow transitioning to a quasi-steady state. In general, the CFD simulations captured the entire initial transient of the flow development properly.

Fig. 6 illustrates the measured and predicted fuel mass per unit volume at 0.1 mm downstream the orifice exits during the quasi-steady-state portion of the injection event. The results were obtained by time-averaging the data from 0.2 to 1.0 ms. The left figure shows the fuel mass per unit volume along the Y axis at $Z = 0$ mm, and the right figure represents the fuel mass per unit volume along the Z axis at $Y = 0$ mm. The results indicated that the simulations performed well in capturing the periphery of the fuel jets. The nozzle flow exhibits strong asymmetrical distribution along the Y axis due to the cavitation in the $Y+$ direction. Along the Z axis, the flow distribution is relatively symmetrical. It is noted that, within the jets, the measured fuel mass per unit volume is lower than the predicted value. The predicted value of around 700 kg/m^3 represents the difference between the densities of the fuel and the am-

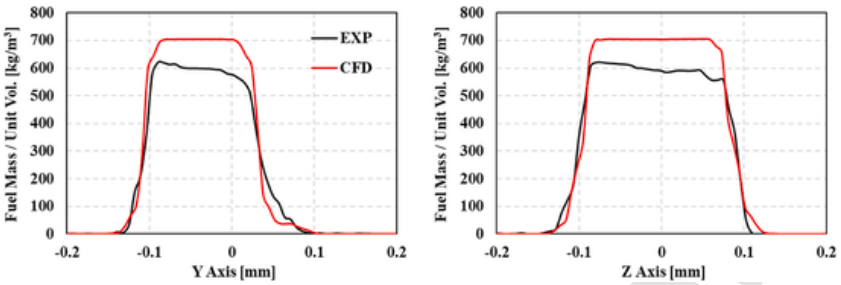

Fig. 6. Measured and predicted fuel mass per unit volume along the Y (left) and Z (right) axes at 0.1 mm from the orifice exit in the quasi-steady stage.

bient gas, which corresponds to the theoretical results of the X-ray measurement. The lower values obtained in the experiments are possibly related to two factors, i.e., the uncertainties in the measurement and the temporal fluctuations of the nozzle flow. The authors carefully examined the raw data of the X-ray measurements and found the temporal fluctuations negligible under this condition. Therefore, it is possible that the measurement uncertainties are responsible for the discrepancy between the simulations and experiments.

In summary, the results shown in this section indicate that the nozzle flow simulations employed in this work performed well in capturing not only the overall flow behavior (e.g., mass flow rate), but also space-resolved characteristics such as the fuel spatial distribution, both in the initial transient and the quasi-steady-state stages. The results provided necessary confidence in the quality of the maps extracted from the in-nozzle flow simulations that were fed to the Lagrangian spray simulations, to be discussed in the next section.

5. Spray simulations

In this section, the Lagrangian spray simulation results obtained with the conventional ROI and the Eulerian-Lagrangian OWC injection modeling approaches are compared. It is noted that the computational setup and all model constants were kept identical for the two cases to guarantee that the differences obtained were solely due to the different parcel initialization methods.

5.1. Spray morphology

Fig. 7 compares the liquid and vapor penetrations from experiments and simulations, which were defined as the farthest axial distance from the orifice exit representing 97% of the liquid-phase fuel, and the farthest point where the local gaseous fuel mass fraction becomes lower than 0.1%, respectively. The experimental data were obtained from the ECN website (2023), with the standard deviation marked by the gray bars. It is shown the liquid length increased sharply and then became relatively stable at around 20 mm in the experiments, which was well captured by the OWC model. In contrast, the ROI model worked well in the initial transient stage, but underpredicted the steady-state liquid length, indicating faster evaporation. In terms of vapor penetration, a typical two-stage development can be identified in the experiments, as described by Hiroyasu and Arai (1990), which was accurately reproduced by both the OWC and ROI models, although the OWC model performed slightly better.

Fig. 8 shows a comparison of the measured and predicted spray plume morphology at different timings. The experimental data corresponds to the schlieren images reported on the ECN website (2023) which identify the periphery of the spray plumes, either in the liquid or vapor phase. In the simulations, the fuel vapor mass fraction was used to represent the spray plume morphology. Note that schlieren imaging is a line-of-sight technique and a projection view is shown, while sliced results across the injector axis were presented in the simulations. Therefore, the results shown in Fig. 8 only provide a reference for qualitative comparison.

At the early stage of injection (0.2 ms), both the ROI and OWC models predicted lower spray spreading angles and longer vapor penetrations compared to the experiments. As the injection continued, the spreading angle in the simulations increased in both cases and became comparable to the experimental results. It is noted that, in the ROI simulations, considerable vapor generation was ob-

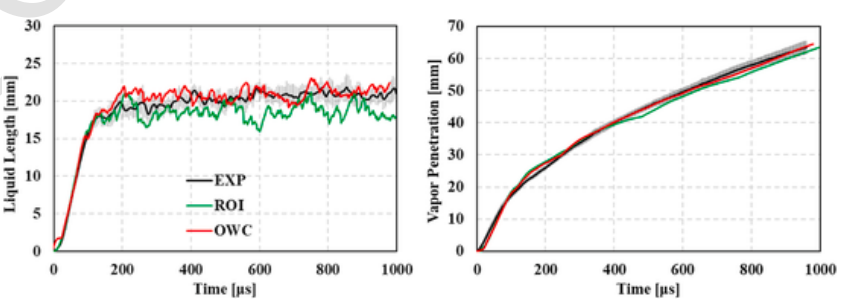

Fig. 7. A comparison of measured and predicted liquid length (left) and vapor penetration (right) under the evaporative condition of 900 K and 6.0 MPa.

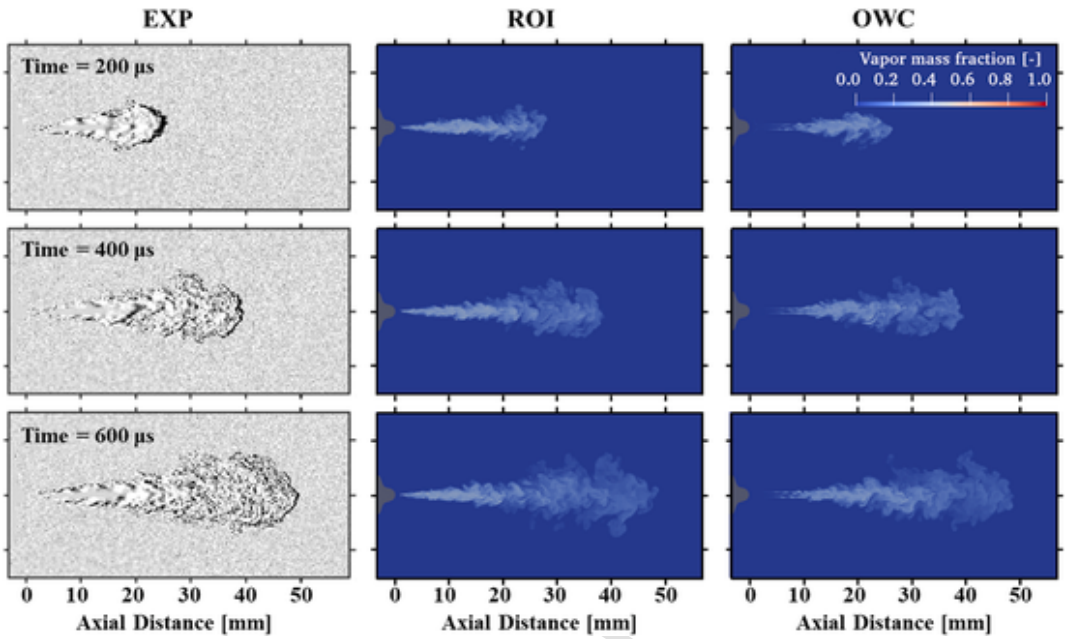

Fig. 8. A comparison of measured and predicted spray plume morphology at different timings under the evaporative condition of 900 K and 6 MPa.

served close to the orifice exit (~1.0 mm) with a conical shape in the near-nozzle region. In contrast, with OWC, vaporization started farther from the orifice exit (~3.0 mm), and it only occurred at the periphery of the plumes. This difference is believed to be the cause of the lower liquid length predicted by the ROI approach, as illustrated in Fig. 7. In general, the predictions from the OWC approach align better with the expected physics because most evaporation occurs in the mixing region between the liquid fuel spray and the ambient gas, which corresponds to the periphery of the spray plumes.

5.2. Mixing-related characteristics

In order to explain the different model predictions presented in Fig. 8, the spatial distribution of fuel mass per unit volume at 5.0 mm downstream of the orifice exits from experiments (Sforzo et al., 2019) and simulations are shown in Fig. 9. Both the experimental and simulation results were obtained by time-averaging the data from 0.6 ms to 1.0 ms to represent the quasi-steady state. In the experiments, significant asymmetry can be found along the Y axis, as the fuel mass per unit volume is much higher in the Y- direction compared to the Y+ direction. This trend is reproduced by the OWC model, as the predictions of the model matched well with the experimental results in both Y and Z directions. In contrast, no asymmetry was predicted by the ROI model, as it should be expected due to the lack of asymmetry in the imposed boundary conditions. Moreover, the predicted fuel mass per unit volume is much lower compared to the experimental value. The results indicate that the OWC approach performed much better than the ROI approach in the near-nozzle region. Besides, the significantly higher liquid fuel concentration near the injector axis explains the lower evaporation in the near-nozzle area, especially within the spray, as predicted by the OWC model.

The discussion above mostly focused on the near-nozzle region within 20 mm from the orifice exit. To examine the models' performance in the far-field, a comparison of the equivalence ratio along the injector axis from a 1-D model and the CFD simulations is shown in Fig. 10. The equivalence ratio is the ratio of fuel mass to oxygen mass divided by the same ratio at stoichiometric condition. The baseline data was calculated by the 1-D spray model described by Musculus and Kattke (2009). It is found that the ROI and OWC

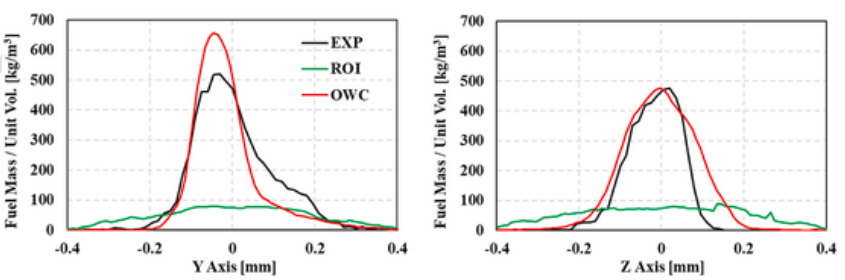

Fig. 9. Measured and predicted fuel mass per unit volume along the Y (left) and Z (right) axes at 5.0 mm from the orifice exit.

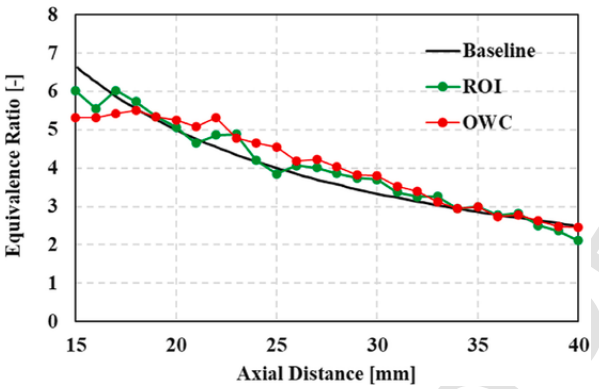

Fig. 10. Predicted equivalence ratio by 1-D model and simulations along the injector axis.

methods predicted similar equivalence ratios along the injector axis beginning at 20 mm from the orifice exit, which is generally consistent with the baseline.

Fig. 11 shows a comparison of the measured and predicted mixture fraction along the radial direction at 40 mm from the orifice exits. The spray asymmetry in the near-nozzle region generally disappeared in the far field, as the distribution of mixture fraction are comparable in all four directions (Y+, Y-, Z+, and Z-). Besides, the difference between the predictions of the two models is much reduced, compared to the near-nozzle region. The results indicate that although the OWC approach showed undoubtedly better performance in dealing with the spray characteristics near the nozzle (< 20 mm), the effect of the in-nozzle flow became weaker in the far-field. This is because the turbulence mixing effect became the dominant aspect as the spray penetrated within the chamber and interacted with the ambient gas. On the other hand, the results also suggested that the conventional ROI approach can be used as a reliable injection modeling method if the near-nozzle spray characteristics are not of interest, which is consistent with the study of Bao et al. (2022).

6. Conclusions

In this study, CFD simulations were performed to study the effect of in-nozzle flow cavitation on the development of the ensuing spray using the ECN Spray C injector. Eulerian simulations of the in-nozzle flow were carried out first to provide accurate flow information at the injector orifice exit. The time- and space-resolved flow characteristics were then employed in the Lagrangian spray simulations via a one-way static coupling approach. The results from the one-way coupling (OWC) approach were compared to that from the conventional rate-of-injection (ROI) approach. The key take-away points are summarized as follows:

1. With regard to the in-nozzle flow simulations, the minimum needle lift and the initial gas volume fraction in the sac and the orifice had considerable effects on the prediction of the initial transient process of the injection event during the needle opening phase. A simulation best practice was developed to capture the transient and quasi-steady-state mass flow rate correctly. The simulations accurately reproduced the time- and space-resolved flow characteristics at the orifice exit, providing necessary confidence in the flow field maps extracted at the orifice exit to be used with the Lagrangian spray simulations.
2. Both the OWC and ROI models performed well in capturing the vapor penetration and spray plume morphology. In the near-nozzle region, considerable evaporation was observed within the plumes with the ROI approach, starting at ~1.0 mm downstream of the orifice exit. In contrast, the evidence of evaporation was found farther away from the orifice exit (~3.0 mm) with the OWC approach, and it only occurred at the plume peripheries, which aligns better with the expected physics.
3. The different performance between the OWC and ROI models in the near-nozzle region is majorly related to the fuel mass distribution. Significantly higher liquid fuel concentration near the injector axis was predicted by the OWC approach, which

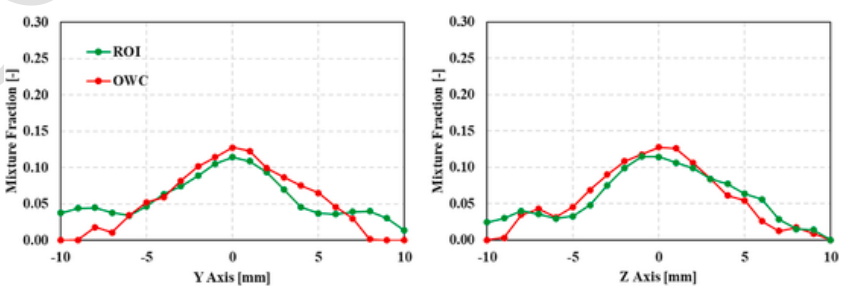

Fig. 11. Predicted mixture fraction along the Y (left) and Z (right) axes at 40 mm from the orifice exit.

matched well with experimental data. In contrast, a wider distribution of fuel mass with lower liquid concentration was predicted by the ROI approach, which led to the stronger evaporation observed in the near-nozzle region.

4. In general, the OWC approach showed better performance when dealing with the spray characteristics near the nozzle (<20 mm). However, the effect of the in-nozzle flow becomes weaker downstream as the spray penetrates and interacts more with the ambient gas. As a result, similar results were predicted by the OWC and ROI models in terms of the far-field mixing-related characteristics (>20 mm). This further suggests that the ROI approach can be used as a reliable injection modeling method for combustion-related research, even with such strong in-nozzle cavitating flow as the ECN Spray C, if the focus is not on the near-nozzle characteristics. On the other hand, more work is needed to assess this claim for reacting cases with longer injection, for which combustion is expected to affect the flowfield characteristics while the injection is still taking place.

Declaration of competing interest

The authors declare that they have no known competing financial interests or personal relationships that could have appeared to influence the work reported in this paper.

Data availability

Data will be made available on request.

Acknowledgments

The submitted manuscript has been created by UChicago Argonne, LLC, Operator of Argonne National Laboratory ("Argonne"). Argonne, a U.S. Department of Energy Office of Science laboratory, is operated under Contract No. DE-AC02-06CH11357. The U.S. Government retains for itself, and others acting on its behalf, a paid-up nonexclusive, irrevocable worldwide license in said article to reproduce, prepare derivative works, distribute copies to the public, and perform publicly and display publicly, by or on behalf of the Government. The Department of Energy will provide public access to these results of federally sponsored research in accordance with the DOE Public Access Plan. http://energy.gov/downloads/doe-public-access-plan.

This research was conducted as part of the Co-Optimization of Fuels and Engines (Co-Optima) initiative sponsored by the US Department of Energy Office of Energy Efficiency and Renewable Energy and Bioenergy Technologies and Vehicle Technologies Offices.

The authors wish to thank:

1. Kevin Stork, Gurpreet Singh, and Michael Weismiller, program managers at DOE, for their support.
2. LCRC cluster facilities at Argonne for the computing resources on the Bebop cluster.
3. Convergent Science Inc. for providing the CONVERGE CFD software licenses.

References

Abbasi, T., & Abbasi, S.A. (2011). *Decarbonization of fossil fuels as a strategy to control global warming. Renewable and Sustainable Energy Reviews*, *15*(4), 1828–1834.

Amsden, A.A. (1997). *KIVA3V. A block-structured KIVA program for engines with vertical or canted valves. Los Alamos National Lab. (LANL), Technical Report, LA-13313-MS*.

Amsden, A.A., O'Rourke, P.J., & Butler, T.D. (1989). *KIVA-II: A computer program for chemically reactive flows with sprays. Los Alamos National Lab. (LANL), Technical Report, LA-11560-MS*.

Andriotis, A., Gavaises, M., & Arcoumanis, C. (2008). *Vortex flow and cavitation in diesel injector nozzles. Journal of Fluid Mechanics*, *610*, 195–215.

Baldwin, E.T., Grover, R.O., Jr., Parrish, S.E., et al. (2016). *String flash-boiling in gasoline direct injection simulations with transient needle motion. International Journal of Multiphase Flow*, *87*, 90–101.

Bao, H., Maes, N., Akargun, H.Y., et al. (2022). *Large eddy simulation of cavitation effects on reacting spray flames using FGM and a new dispersion model with multiple realizations. Combustion and Flame*, *236*, 111764.

Battistoni, M., Magnotti, G.M., Genzale, C., et al. (2018). *Experimental and computational investigation of subcritical near-nozzle spray structure and primary atomization in the Engine Combustion Network Spray D. SAE International Journal of Fuels and Lubricants*, *11*(4), 337–352.

Battistoni, M., Som, S., & Powell, C.F. (2019). *Highly resolved Eulerian simulations of fuel spray transients in single and multi-hole injectors: Nozzle flow and near-exit dynamics. Fuel*, *251*, 709–729.

Bilicki, Z., & Kestin, J. (1990). *Physical aspects of the relaxation model in two-phase flow. Proceedings of the Royal Society A*, *428*(1875), 379–397.

Chen, Z., He, Z., Shang, W., et al. (2018). *Experimental study on the effect of nozzle geometry on string cavitation in real-size optical diesel nozzles and spray characteristics. Fuel*, *232*, 562–571.

Downar-Zapolski, P., Bilicki, Z., Bolle, L., et al. (1996). *The non-equilibrium relaxation model for one-dimensional flashing liquid flow. International Journal of Multiphase Flow*, *22*(3), 473–483.

Duan, X., Lai, M.C., Jansons, M., et al. (2021). *A review of controlling strategies of the ignition timing and combustion phase in homogeneous charge compression ignition (HCCI) engine. Fuel*, *285*, 119142.

Dukowicz, J.K. (1980). *A particle-fluid numerical model for liquid sprays. Journal of Computational Physics*, *35*(2), 229–253.

Engine Combustion Network. https://ecn.sandia.gov/diesel-spray-combustion/target-condition/spray-c-nozzle-geometry/. 2023.

Gimeno, J., Bracho, G., Martí-Aldaraví, P., et al. (2016). *Experimental study of the injection conditions influence over n-dodecane and diesel sprays with two ECN single-hole nozzles. Part I: Inert atmosphere. Energy Conversion and Management*, *126*, 1146–1156.

Guo, G., He, Z., Zhang, Z., et al. (2020). *Visual experimental investigations of string cavitation and residual bubbles in the diesel nozzle and effects on initial spray structures. International Journal of Engine Research*, *21*(3), 437–447.

Guo, H., Torelli, R., Rodriguez, A.B., et al. (2020). *Internal nozzle flow simulations of the ECN Spray C injector under realistic operating conditions. SAE International Journal of Advances and Current Practices in Mobility*, *2*(4), 2229–2240.

Hiroyasu, H., & Arai, M. (1990). *Structures of fuel sprays in diesel engines*. SAE Technical Paper, 900475.

Kanda, T., Hakozaki, T., Uchimoto, T., et al. (2005). *PCCI operation with early injection of conventional diesel fuel*. SAE Technical Paper. 2005-01-0378.

Krishnamoorthi, M., Malayalamurthi, R., He, Z., et al. (2019). *A review on low temperature combustion engines: Performance, combustion and emission characteristics. Renewable and Sustainable Energy Reviews*, *116*, 109404.

Leung, J.C. (1986). *A generalized correlation for one-component homogeneous equilibrium flashing choked flow*. *AIChE Journal*, *32*(10), 1743–1746.
Maes, N., Skeen, S.A., Bardi, M., et al. (2020). *Spray penetration, combustion, and soot formation characteristics of the ECN Spray C and Spray D injectors in multiple combustion facilities*. *Applied Thermal Engineering*, *172*, 115136.
Musculus, M.P.B., & Kattke, K. (2009). *Entrainment waves in diesel jets*. *SAE Journal of Engines*, *2*(1), 1170–1193.
Nocivelli, L., Yan, J., Saha, K., et al. (2019). *Effect of ambient pressure on the behavior of single-component fuels in a gasoline multi-hole injector*. ASME Internal Combustion Engine Division Fall Technical Conference, V001T02A012.
Payri, F., Bermúdez, V., Payri, R., et al. (2004). *The influence of cavitation on the internal flow and the spray characteristics in diesel injection nozzles*. *Fuel*, *83*(4–5), 419–431.
Payri, R., Gimeno, J., Cuisano, J., et al. (2016). *Hydraulic characterization of diesel engine single-hole injectors*. *Fuel*, *180*, 357–366.
Peng, Q., Rockstroh, T., & Hall, C. (2022). *The impact of fuel and injection strategy on combustion characteristics, emissions and efficiency in gasoline compression ignition operation*. *Fuel*, *318*, 123548.
Pitz, W.J., & Mueller, C.J. (2011). *Recent progress in the development of diesel surrogate fuels*. *Progress in Energy and Combustion Science*, *37*(3), 330–350.
Pomraning, E. (2001). *Development of large eddy simulation turbulence models* Ph.D. USA: University of Wisconsin-Madison.
Quan, S., Senecal, P.K., Pomraningm, E., et al. (2016). *A one-way coupled volume of fluid and Eulerian-Lagrangian method for simulating sprays*. ASME Internal Combustion Engine Division Fall Technical Conference, V001T06A014.
Redlich, O., & Kwong, J.N.S. (1949). *On the thermodynamics of solutions. V. An equation of state. Fugacities of gaseous solutions*. *Chemical Reviews*, *44*(1), 233–244.
Reitz, R.D. (1987). *Modeling atomization processes in high-pressure vaporizing sprays*. *Atomization and Spray Technology*, *3*, 309–337.
Reitz, R.D., & Beale, J.C. (1999). *Modeling spray atomization with the Kelvin-Helmholtz/Rayleigh-Taylor hybrid model*. *Atomization and Sprays*, *9*(6), 623–650.
Reitz, R.D., & Duraisamy, G. (2015). *Review of high efficiency and clean reactivity controlled compression ignition (RCCI) combustion in internal combustion engines*. *Progress in Energy and Combustion Science*, *46*, 12–71.
Richards, K.J., Senecal, P.K., & Pomraning, E. (2022). *CONVERGE 3.0 manual.* Convergent Science.
Saha, K., Quan, S., Battistoni, M., et al. (2017). *Coupled Eulerian internal nozzle flow and Lagrangian spray simulations for GDI systems*. SAE Technical Paper. 2017-01-0834.
Sforzo, B.A., Tekawade, A., Matusik, K., et al. (2019). *3D measurements of the geometry, internal flow and emerging fuel jet from the ECN Spray C injector*: *Vol. 2019*. ILASS-Europe.
Sou, A., Hosokawa, S., & Tomiyama, A. (2007). *Effects of cavitation in a nozzle on liquid jet atomization*. *International Journal of Heat and Mass Transfer*, *50*(17–18), 3575–3582.
Tekawade, A., Sforzo, B.A., Matusik, K.E., et al. (2020). *Time-resolved 3D imaging of two-phase fluid flow inside a steel fuel injector using synchrotron X-ray tomography*. *Scientific Reports*, *10*(1), 8674.
Torelli, R., Pei, Y., Zhang, Y., et al. (2022). *End-to-end modeling of fuel injection via static coupling of internal flow and ensuing spray*. *Communications Engineer*, *1*(1), 42.
Yao, M., Zheng, Z., & Liu, H. (2009). *Progress and recent trends in homogeneous charge compression ignition (HCCI) engines*. *Progress in Energy and Combustion Science*, *35*(5), 398–437.